Available online at www.sciencedirect.com
SCIENCE DIRECT®
PERGAMON
International Journal of Heat and Mass Transfer 46 (2003) 2279–2290
International Journal of HEAT and MASS TRANSFER
www.elsevier.com/locate/ijhmt

Mist/steam cooling by a row of impinging jets

X. Li [a], J.L. Gaddis [b], T. Wang [a,*]

[a] *Energy Conversion and Conservation Center, University of New Orleans, 932 Engineering Building, New Orleans, LA 70148-2220, USA*

[b] *Department of Mechanical Engineering, Clemson University, Clemson, SC 29634-0921, USA*

Received 7 March 2002; received in revised form 13 September 2002

Abstract

Mist/steam cooling has been studied to augment internal steam-only cooling for advanced turbine systems. Water droplets generally less than 10 μm are added to 1.3 bar steam and injected through a row of four round jets onto a heated surface. The Reynolds number is varied from 7500 to 22,500 and the heat flux varied from 3.3 to 13.4 kW/m^2. The mist enhances the heat transfer along the stagnation line and downstream wanes in about 3 jet diameters. The heat transfer coefficient improves by 50–700% at the stagnation line for mist concentrations 0.75–3.5% by weight. Off-axis maximum cooling occurs in most of the mist/steam flow but not in the steam-only flow. CFD simulation indicates that this off-axis cooling peak is caused by droplets' interaction with the target walls.

Keywords: Impinging jets; Mist cooling; Two-phase flow; Heat transfer enhancement

1. Introduction

Current heavy frame advanced turbine systems (ATS) are being developed using steam as the coolant for the blades. In this approach, the loss of energy to coolant can represent a gain in the energy supplied to the bottom cycle and is partially retrieved as work. The encouragement of higher turbine inlet temperature to increase thermal efficiency will continue to challenge designers to improve airfoil internal cooling. With the advent of single crystal blades of superalloys, the difficulty of forming the internal passages is of concern. Particularly, addition of internal ribs or surface contours to boost heat transfer coefficients in a single crystal blade is an expensive process. The concept of mist cooling investigated in this paper is believed to have the potential of significantly enhancing the cooling effectiveness without resorting to internal ribs or turbulators. Hence, a less expensive blade passage can be used. Furthermore, with enhanced internal cooling, the required mass flow rate of cooling steam can be reduced. This would result in reduced pressure losses and increased bottom cycle efficiency. The advantages and reasons of using mist/steam cooling, a comparison of mist/air and mist/steam cooling, and a review of previous related studies have been presented by Guo et al. [1].

Guo et al. [1] explored mist in a straight tube, then extended the testing to a 180° bend [2]. They demonstrated average enhancement of over 100%, with the highest local cooling enhancement of 200%, by employing less than 5% mist (by weight) for the straight tube. In the bent tube overall cooling enhancements ranged from 40% to 300% with the maximum local cooling enhancement being over 800% for both inner and outer tube bend surfaces.

Single-phase jet impingement has been studied extensively, including heat transfer at the stagnation point, local heat transfer and effects of turbulence intensity and nozzle geometry. However, few studies have been found on mist jet impingement. Li et al. [3] addressed a flat surface impacted by a two-dimensional slot jet of mist. They demonstrated over 100% cooling enhancement at the stagnation point with 1.5% mist.

Nirmalan et al. [4] conducted an experimental study of turbine vane heat transfer with water–air mist cooling.

* Corresponding author. Tel.: +1-504-280-7183; fax: +1-504-280-5539.
E-mail address: twang@uno.edu (T. Wang).

0017-9310/03/$ - see front matter
doi:10.1016/S0017-9310(02)00521-5

Nomenclature

d	jet diameter, m	q''	heat flux, W/m^2
h	heat transfer coefficient, W/m^2 K	T_w	wall temperature, K
h_0	heat transfer coefficient with steam alone	T_{sat}	saturation temperature, K
h_{mist}	heat transfer coefficient with mist/steam	x	position from stagnation line, m
m_l/m_s	mass concentration of mist in steam		
Re	Reynolds number, Vd/v	*Greek symbol*	
V, V_{jet}	jet velocity, m/s	v	kinematic viscosity, m^2/s

Water was pressured inside the vane and broken up into small droplets through many cooling holes on an inner wall inside the vane and impinged on the inner side of the vane's outer wall. Their results showed significant cooling enhancement using water/air mist jets, but they found the jets are difficult to control and resulted in non-uniform overcooling over the target surface. A literature review of jet impingement heat transfer in mist/air stream by Goodyer and Waterston [5], Takagi and Ogasawara [6], Mastanaiah and Ganic [7] and Fujimoto and Hatta [8] was conducted by Li et al. [3] and is not repeated here. More detailed literature review of mist cooling and impingement jet cooling including the effects of target distance, turbulence levels, etc. can be found in [9].

2. Background information

To provide some background information for analyzing the results of the present study, the modeling of mist cooling enhancement mechanisms by Li et al. [10] is briefed below.

They proposed that the mist/steam jet impingement heat transfer could be due to four identified mechanisms: an ordinary single phase effect, modifications to the flow of the single phase by the mist, quenching of the thermal boundary layer by the mist, and direct contact of mist droplets with the surface. To model each of these mechanisms, they specifically considered.

2.1. Heat transfer from the target wall to the steam

Heat transfer due to the steam is modeled as heat convection of a single-phase steam flow. The heat transfer enhancement through the effect of droplets on the flow has been assumed to be of secondary importance. Experimental study by Yoshida et al. [11] found 170% enhancement by adding 80% by mass glass beads of diameter 50 μm to the airflow. Considering the effect of the particles includes boundary layer disturbance as well as other cooling effects in the present study with less than 5% water droplets, the enhancement of the single-phase heat transfer due to droplets on the flow is projected to be less than 4%.

2.2. Heat transfer between the droplet and steam (or quenching effect)

Heat transfer between the droplets and steam represents the quench effect due to water droplets, and it can be modeled by considering droplets as a distributed heat sink. The droplets evaporate into the superheated steam inside the thermal boundary layer and quench the boundary layer. Li et al. [10] employed a superposition model to calculate the heat transfer between droplets and steam by dividing the temperature of mist/steam flow into two parts, $T = T_1 + T_2$. T_1 is the temperature of steam-only flow and T_2 is the temperature depression caused by the mist.

2.3. Heat transfer from the target wall to droplets (or direct contact cooling)

Unlike spray cooling, where the droplet momentum is supplied by a device, small mist droplets may not be able to hit the wall because of the drag force in the present study. Based on trajectory analysis by Wang et al. [9], it is believed that larger droplets will hit the wall if the approach velocity is high enough. Though neglected in trajectory analysis herein, the droplets are subject to a lift "force" due to the momentum imbalance of asymmetric evaporation.

According to Buyevich and Mankevich [12], the droplet will depart from (or bounce off) the wall if the impact velocity is lower than a critical velocity when the surface is superheated above 30 °C. Heat transfer from the wall to the droplet will pass through a vapor layer for non-sticking droplets.

Once a droplet hits the wall, whether it rebounds from the wall depends on the wall temperature, the impact velocity, and the *residence time* of the droplet, which is the time elapsed for a droplet staying on the wall momentarily until it reaches some superheat on the wall. The residence time is affected by wall superheat, surface tension, impact velocity, and thermodynamic properties.

Typically, a high wall temperature will reject the droplet after a short time while a low wall temperature will permit the droplet to remain much longer. Li et al. [10] applied a transient conduction model of a spherical cap geometry of a water droplet for a residence time to analyze the *direct contact cooling* of a single water droplet. The residence time was longer than that proposed by Hatta et al. [13] for much higher temperatures. Li's data demand that the contact time with the wall be inversely related to the wall temperature.

To predict the overall heat transfer by direct contact of those droplets that contact the wall, one must calculate trajectories for the droplets and the droplet mass flow rate to the wall. The commercial code FLUENT [14] was employed to compute two-phase particle-laden flows.

Based on the experimental results of a slot impinging jet from [3,16], with effects of mist experimentally observed to be multiples of the single-phase heat transfer, it is evident that the direct contact of droplets is the primary enhancement mechanism. After a detailed modeling of each heat transfer mechanism, Li et al. [10] further argued that the evaporation of liquid is limited to a small percent of the total mist. The model of Buyevich and Mankevich [12,15], which would have a fraction of contacting droplets stick and evaporate completely, was rejected because the observed heat flows were too low to have more than a tiny fraction of droplets evaporate completely.

Using the contact time and contact area as described above and droplet impact densities calculated using FLUENT, the modeling successfully calculated the heat flow within 7% of Li's [16] experimental data. The results of modeling also indicate that direct contact of droplets indeed is the primary enhancement mechanism and the quenching effect is relatively minor. The single-phase steam convection is proportional to temperature difference and the direct contact cooling is more nearly constant. Therefore the direct cooling component will be a lower portion of the total as heat flux increases. For example from [10] at constant flow conditions, as the surface heat flux is increased by 78% the steam convective cooling increases from 41% to 55%, whereas the mist direct cooling decreases from 57% to 42%. The remaining 2–3% are the quenching effect. This above background information is essential for interpreting the present data.

3. Experimental facility

Fig. 1a shows a cross-sectional view of the test section. Steam or steam with mist enters from the supply at the top into a settling chamber and passes through four in-line holes and onto the heated surface. Five heater segments, as shown in Fig. 1b are arranged electrically in series in serpentine form and powered by a low-voltage DC external power supply. Type K thermocouples are located on two rows: one in line with a jet and one along a line between jets. The thermocouples are inserted through a hole in the ceramic backing plate; laid for 50 diameters on a line parallel with the jet centerlines; and are electrically insulated from the heater surfaces by a mica sheet (Cogebi). Additional details of the heater material and resistance are provided in [3]. Transparent sidewalls allow viewing the surface and obtaining optical information. The flow exits into chambers on the left and right.

The jets have a rounded entry contour and a diameter of 8.1 mm. The jets are spaced laterally by 25 mm and the jet surface plate is spaced 22.5 mm from the heated section. The steam and mist is supplied at a pressure of about 1.3 bar at 103–104 °C from a mixing chamber where saturated steam and liquid mist are blended. The mixing chamber (not shown) is more than one meter above the test section allowing thermal accommodation of the droplets. The supply system is fitted with several liquid traps positioned at strategic positions to allow mass balances to be performed. The method of catch and weigh has been employed and found to be superior to mass flow instrumentation, though still subject to uncertainty.

The detailed steam supply and mist generating systems were described by Guo et al. [1] and Li et al. [3]. Fig. 2 gives the layout of the experimental system and a brief summary of the system is followed. The mist was generated from filtered water using mist-generating nozzles (donated by Mee Industries Inc.), which direct a small jet onto the point of a cone. The nozzles were supplied at 1000 psi. The nozzles were located in the mixing chamber through which the steam also passed. The exit of the mixing chamber and the delivery tube used in both this experiment and [1] was surveyed by an Aerometrics phase Doppler particle analyzer. The water droplet size ranged from 2 to 9 μm with a few droplets observed at 15 μm. The arithmetic mean size was 3.2 and the volume average mean size 5.3 μm. The analyzer did not observe droplets below 2 μm. The modeling of [10] indicated that any smaller droplets, including those below 4 μm have a diminished importance to the enhancement. The characteristics and statistics of the droplet size and velocity distributions have been documented previously in [1,3].

Data were obtained for the temperature distribution of the surface with and without mist at various Reynolds numbers, heat fluxes and mist concentrations. The procedure generally followed was to set the steam flow and the electric current and take a set of data, including the mass flow rates at each exit. Then, the liquid mist is added without changing the vapor flow. Adding mist reduces the vapor flow by an amount required to heat the liquid to saturation, of the order of a percent. The

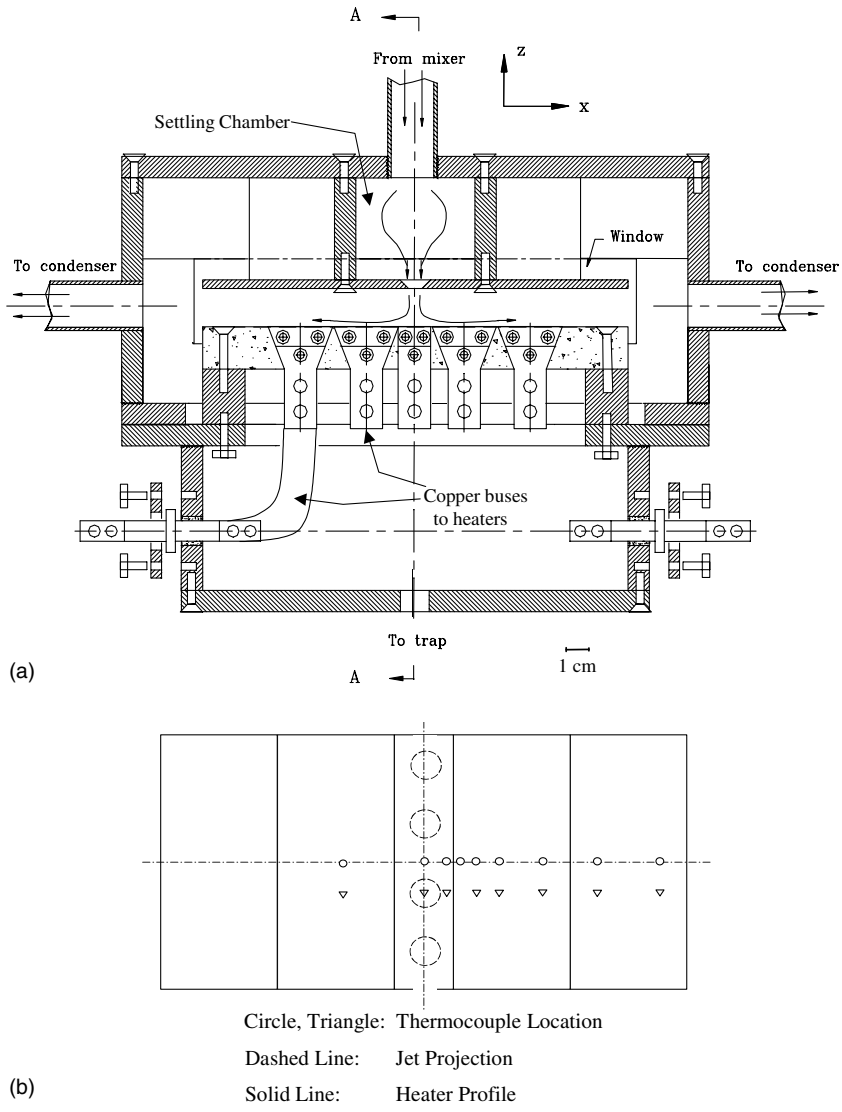

Fig. 1. Schematic of the test section (a), cross-section of the test article (b), and top view of the target surface.

procedure allows the mass flow change as a sole result of adding the mist. Dependence is placed on the steadiness of the flows and heat losses. Data reduction procedures include thermocouple calibration correction, the effect of temperature on resistivity of the heater elements, the backside heat loss, and compensation for small flow variations due to steam used to remove subcooling of the injected mist.

3.1. Uncertainty analysis

An uncertainty analysis has been performed based on the methods of Moffat [17]. An Nth-order analysis has been performed on both heat transfer and flow. The sources of uncertainty are temperature, flow mass, mass collection time, property valuation, heater current (voltage across shunt), and dimensions. Uncertainty in temperatures is within 0.5 °C. For the Reynolds number and primary steam flow rates, the uncertainty is small, less than 2%. The mist mass is determined by mass collection and subtraction such that the collection time has the largest influence and the uncertainty is about 20%. For the heat transfer coefficient, the largest source of uncertainty is the shunt voltage reading. The uncertainty in heat transfer rate is 5.5% at the highest heat flux, increasing to double that at low heat flux. Thus the uncertainty in heat transfer coefficient is slightly higher due to the uncertainty of temperature, a net of 6.3% at the highest heat flux. The detailed uncertainty analysis is documented in [9].

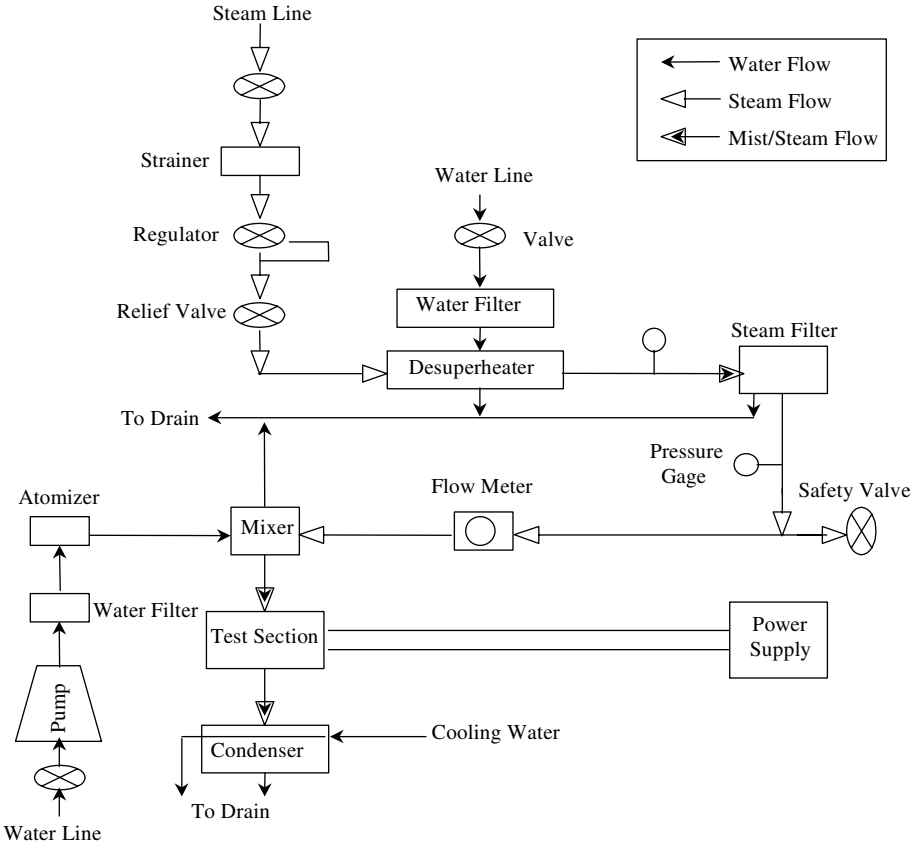

Fig. 2. Schematic of the experimental system.

4. Results and discussion

Fig. 3a shows the temperature distribution obtained at jet Reynolds number = 15,000, heat flux = 7540 W/m^2, and mist concentration 1.5%, together with the data for steam alone at the same Reynolds number and heat flux. It is obvious that the addition of mist lowers the temperature substantially in the impact zone of the jets. Also, as would be anticipated, the temperature drop wanes in the region removed from the jet impact. The point with lowest wall temperature is actually at a position off the jet centerline by about one diameter on each row of thermocouples. The heat transfer coefficient, h, is defined as

$$h = \frac{q''}{T_w - T_{sat}}. \quad (1)$$

The choice of T_{sat} could have been T_{jet} in this definition, as is conventional in jet impingement heat transfer studies. In this study the jet is at saturation conditions. Use of Eq. (1) with the data of Fig. 3a allows the heat transfer coefficients of Fig. 3b to be produced.

As is clear from the data, the mist provides a heat transfer coefficient up to about 4 times as large as h_0, the single-phase heat transfer coefficient, near the impact zone of the target surface. The enhancement, defined as h_{mist}/h_0 and plotted in Fig. 3c, declines in the region away from the impact zone to a negligible enhancement for $x/d > 5$. It is obvious to see that the maximum cooling effect for the mist case in Fig. 3b is not located at the stagnation region, whereas the steam-only case preserves a nearly constant heat transfer rate within one-diameter distance from the stagnation region. This offset cooling maximum is not due to measurement uncertainty or property variations, but it is real. The physical mechanism will be discussed in detail later.

Figs. 4 and 5 indicate the effect of heat flux at the same mist concentration and Reynolds number. Fig. 4 has a higher heat flux and Fig. 5 has a lower heat flux. There are several items of note. The stagnation region ($x = 0$) heat transfer coefficient for steam alone increases with heat flux. Principally this effect is attributed to thermal property variation with temperature. If the heat transfer coefficients are converted to Nusselt number by using the thermal conductivity evaluated at the mean of jet and surface temperature, it can be revealed that the Nusselt number (shown in Fig. A.1 in the Appendix A) at $x = 0$ is nearly constant for various heat fluxes when the Reynolds number is the same. The temperature

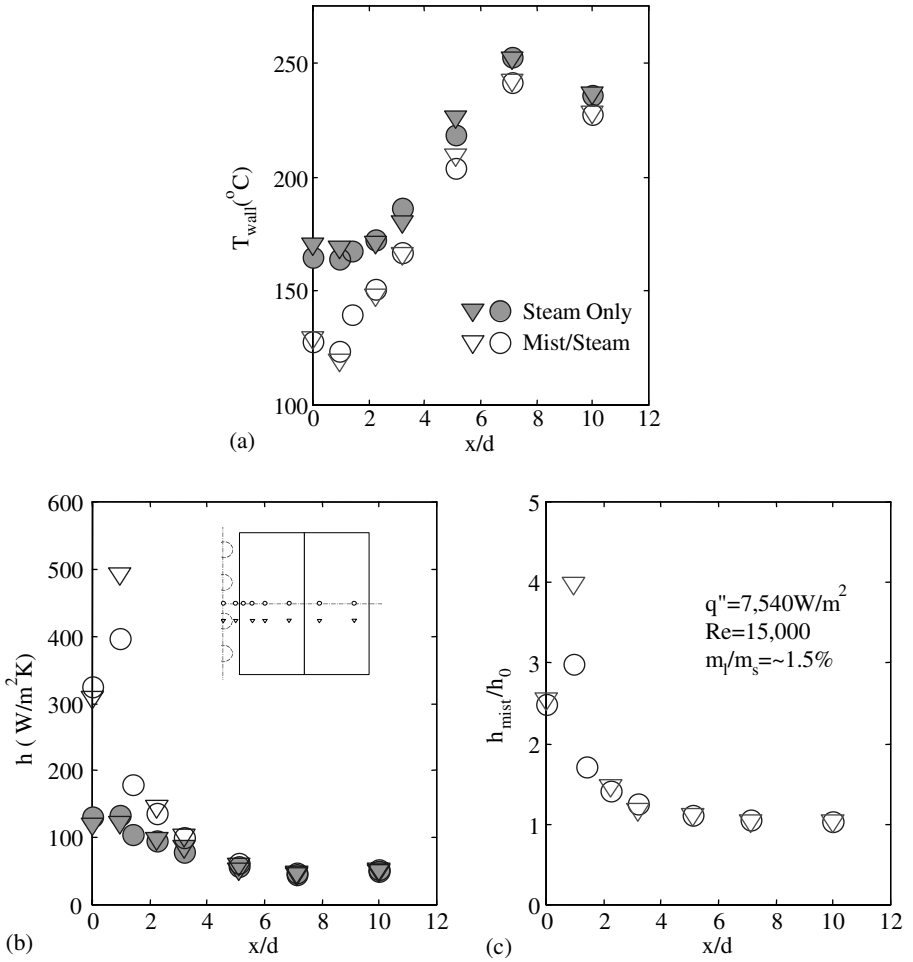

Fig. 3. Typical heat transfer result of mist/steam jet impingement ($q'' = 7540$ W/m^2, $Re = 15{,}000$, $m_l/m_s = \sim 1.5\%$): (a) wall temperature, (b) heat transfer coefficient and (c) ratio of heat transfer coefficient (enhancement).

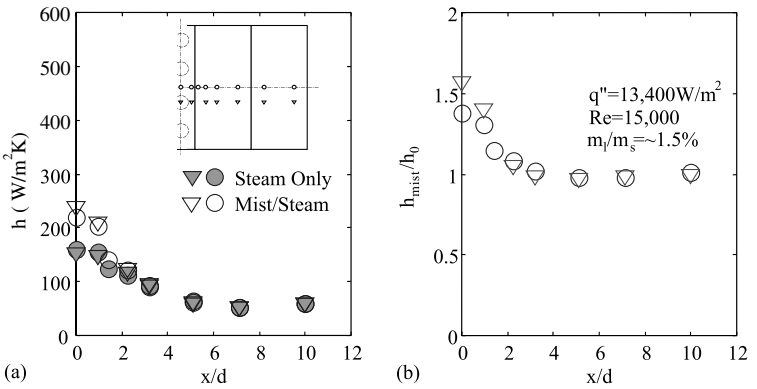

Fig. 4. Heat transfer results ($q'' = 13,400$ W/m^2, $Re = 15{,}000$, $m_l/m_s = \sim 1.5\%$): (a) heat transfer coefficient and (b) ratio of heat transfer coefficient (enhancement).

distributions in line with the injection holes and between injection holes are highly similar. With the spacing of the jets from the plate of approximately three diameters and the impinging distance of 2.8 diameters, the cooling ef-

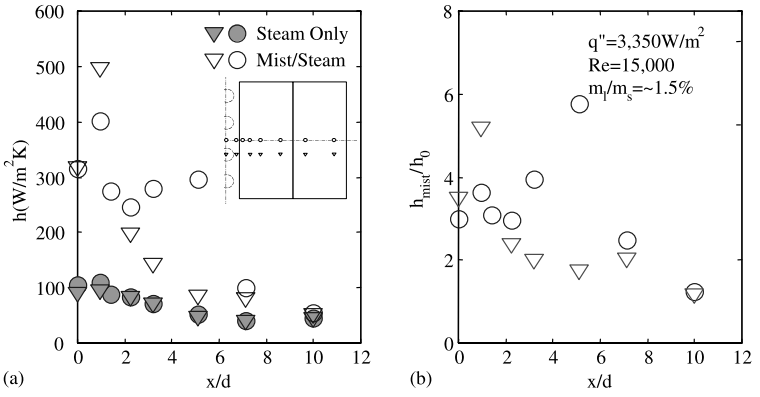

Fig. 5. Heat transfer results ($q'' = 3350$ W/m^2, $Re = 15{,}000$, $m_l/m_s = \sim 1.5\%$): (a) heat transfer coefficient and (b) ratio of heat transfer coefficient (enhancement).

fect is quite uniform spanwise as indicated by the instrumented locations.

The power of mist to reduce temperature is comparatively greater at lower heat flux than at higher heating. The principal reason is that the direct droplet contact cooling, as discussed in Section 2, presumably increases slightly as the temperature decreases while the total heating is reduced. The total heat flux declines essentially fourfold between Figs. 4 and 5. Therefore when the enhancement, h_{mist}/h_0, reaches 1.5 at high heat flux in Fig. 4b the direct impact cooling may account for up to one-third of the cooling, or about 4400 W/m^2. When the total heat flux drops to 3350 W/m^2, the direct contact cooling may obviously account for all the cooling. Continued reduction in heat application is expected to result in flooding (or wetting) of the target surface. At the points of $x/d = 3$ and 5 for the low heat flux in Fig. 5, there is an extreme effect of local cooling enhancement by the mist. It seems to be out of the trend, and may reflect upstream flooding. Not shown in the paper is that the temperature elevation of all the first five positions lie in the narrow range of 11–14 °C above saturation temperature. At this temperature range the expected mode of heat flow would be simple evaporation with possibly some augmentation due to nucleation within any film. Under the hypothesis of flooding, the predicted film thickness is between 10 and 15 μm, which is undetectable by normal vision. Although flooding was never observed by naked eye during the experiment, it is suspected that flooding of the surface has occurred. It seems that the film spreads under the influence of shear and that the film extends further on the device centerline than in line with one of the holes. On the centerline (circles) the film seems to extend past $x/d = 5$ but not to $x/d = 7$; in line with a hole (triangles) the film extends only to $x/d = 3$ and not to $x/d = 5$. Because of the direction of shear away from the holes, thinning should be expected in line with the hole and relative thickening along the line between holes where liquid films converge and accumulate. However, in Fig. 5 there is still a cooling enhancement far downstream of the jets at $x/d = 8$. At both the intermediate (Fig. 3) and high heat flux (Fig. 4), the enhanced cooling effect has essentially waned by $x/d = 3$. The results presented in Nusselt number in Appendix A allow us make more comparisons but the conclusions are consistent with what are talked here.

Figs. 6–8 show the low, medium, and high heat flux results at Reynolds number 22,500 and 0.75% mist concentration. Although the same supplying nozzle system was used to produce mist, the mist mass flow is a little bit lower than that at the Reynolds number 15,000 and 1.5% mist concentration. The reason is that there is more droplet attrition in transit at higher Reynolds number (higher velocity). All heat transfer rates are increased at the higher velocity. Mist enhancements of 1.5–7 folds near injection positions wane to negligible effect by about $x/d = 3$. Not as the case $Re = 15{,}000$ (Fig. 5) however, at $Re = 22{,}500$ no points has been found out of the trend at the lowest heat flux, which may be due to the lower mist concentration. All other features from the earlier discussion are observed in this data cluster.

Figs. 9 and 10 indicate the data achieved with a lower steam flow, at Reynolds number = 7500. Here, only two heat flux levels are reported. The same patterns are definitely indicated. Lower overall heat transfer coefficients are observed and they depend slightly on the temperature level. The injection region has higher heat transfer coefficients and higher enhancement. The temperature traces in line with a hole and between holes are quite uniform. The lowest temperature occurs at $x/d \sim 1$ for both rows of instrumentation. The mist forms a larger concentration in the reduced steam flow and enhancements of nearly eightfolds are realized.

As little as 0.75% mist is uniformly capable of providing 50% or more stagnation-point enhancement at the worst observed conditions. This powerful effect summarizes the potency of the mist cooling for situations

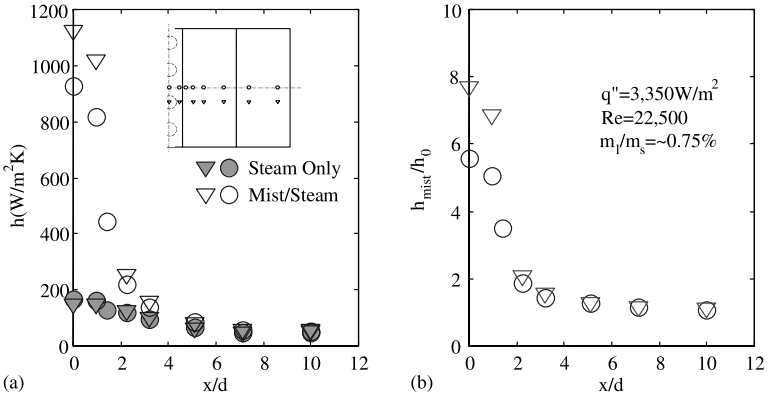

Fig. 6. Heat transfer results ($q'' = 3350$ W/m^2, $Re = 22{,}500$, $m_l/m_s = \sim 0.75\%$): (a) heat transfer coefficient and (b) ratio of heat transfer coefficient (enhancement).

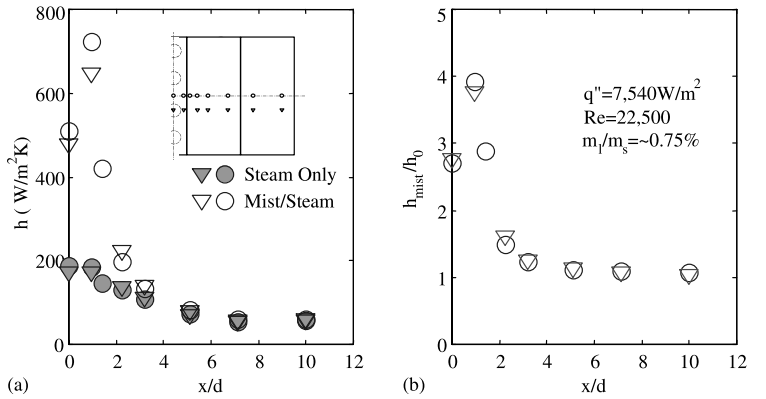

Fig. 7. Heat transfer results ($q'' = 7540$ W/m^2, $Re = 22{,}500$, $m_l/m_s = \sim 0.75\%$): (a) heat transfer coefficient and (b) ratio of heat transfer coefficient (enhancement).

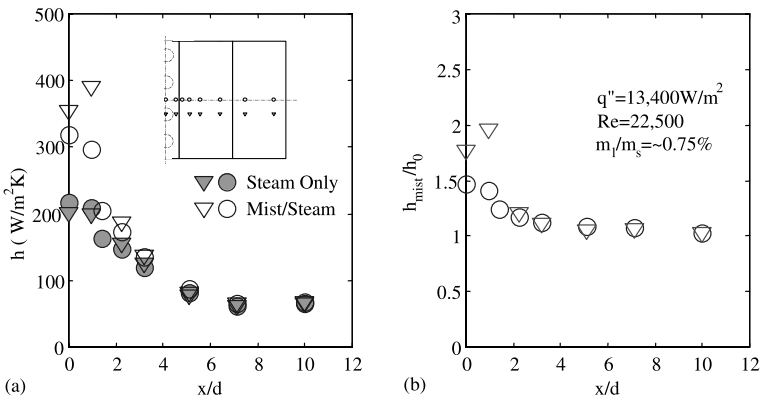

Fig. 8. Heat transfer results ($q'' = 13{,}400$ W/m^2, $Re = 22{,}500$, $m_l/m_s = \sim 0.75\%$): (a) heat transfer coefficient and (b) ratio of heat transfer coefficient (enhancement).

having direct impact of fluid on the heated surface. Farther downstream, the effect wanes. The details of this waning effect are dependent on the conditions of the experiment.

4.1. Comparison with the slot jet

It is of interest to compare the present results with those of the slot jet reported in Li et al. [3] in the same

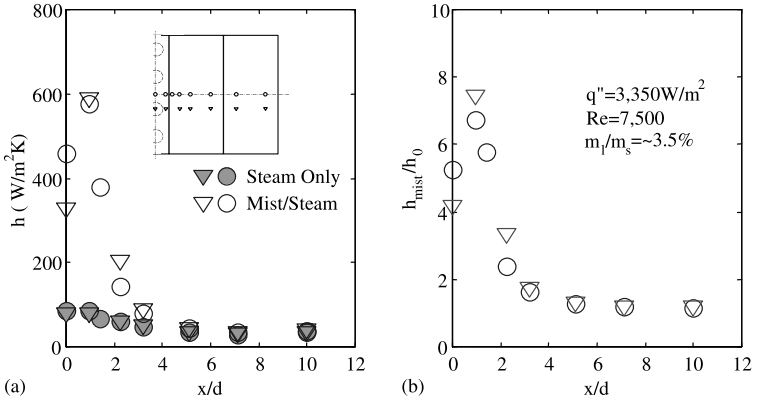

Fig. 9. Heat transfer results ($q'' = 3350$ W/m^2, $Re = 7500$, $m_l/m_s = \sim 3.5\%$): (a) heat transfer coefficient and (b) ratio of heat transfer coefficient (enhancement).

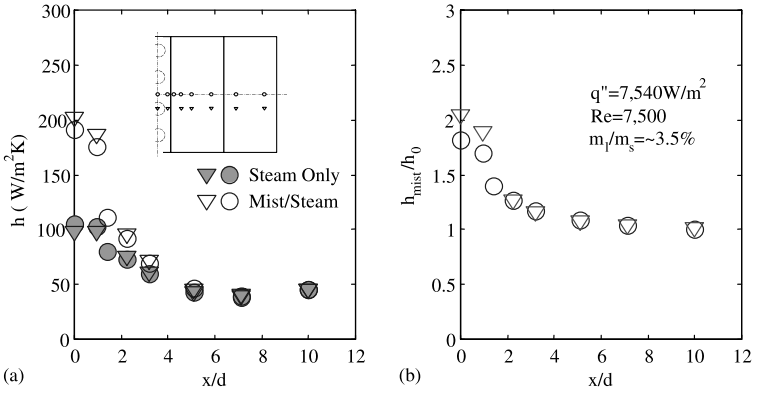

Fig. 10. Heat transfer results ($q'' = 7540$ W/m^2, $Re = 7500$, $m_l/m_s = \sim 3.5\%$): (a) heat transfer coefficient and (b) ratio of heat transfer coefficient (enhancement).

cavity. The fairest way to compare the results is at equal mass flow rates rather than at the same Reynolds number. The mass flow rate in the present study with a row of four holes is approximately 54% of that of the slot jet of the same Reynolds number. Note that the Reynolds number in the slot jet study is based on twice that of the slot width. Therefore, the $Re = 7500$ in the current experiment has a mass flow near but above the $Re = 14{,}000$ of the slot in [3]. If Fig. 10 in this paper is compared with the corresponding case in Fig. 7 of Li et al. [3] (or Fig. A.2 in this paper) at the same Reynolds number, mist ratio, and wall heat flux, it can be seen that the steam-only case has similar h-values while the maximum mist/steam h-value of the slot jet is approximately 1.4 times that of round jets' maximum mist h-value. Since the mass flow rates of the slot jet is approximately twice that of the four round jets of the same Reynolds number, it can be deduced that a row of four round jets give superior cooling in the steam-only case, whereas the slot jet performs better on mist/steam enhancement.

4.2. Discussion of off-axis maximum cooling

In both the previous study of a slot jet and the present study of a row of four round jets, the off-axis maximum cooling occurs in most of the mist/steam cases, but in none of the steam-only cases. Therefore, the authors believe this is the consequence of droplet dynamics. Potential instrumentation errors and measuring uncertainties have been examined, but nothing can contribute to the magnitude comparable to the significant enhancement as shown in the data. For example, a temperature difference of 5 °C across the heater in Fig. 1 will only contribute to a negligible value of 0.19% of the heat flux value.

To perform a quick and simple simulation of droplet dynamics to aid in interpreting the off-axis cooling peaks, the commercial code FLUENT [14] is employed. A 2-D simulation is conducted to relate qualitatively to the actual 3-D situation. The droplets are computed as a separable phase having momentum interchange with the stream phase. Drag of the droplets in proportion to the

slip between steam and droplet velocity is considered. The droplets are placed uniformly at 100 equally spaced positions at the jet entrance. Since the droplet concentration is low, the momentum of the flow is dominated by the steam (gas) phase. The grid independence and the turbulent model fidelity are checked by comparison with actual heat transfer results. Detail discussion of this computation can be found in [16].

Fig. 11a shows the computed droplet trajectory for two different sizes. The computed result of density of impact normalized by the density in the incoming jet is shown in Fig. 11b for the three velocities studied. Clearly the droplets spread more at lower jet velocity and there is a depleted impact density at the centerline due to the spreading. Fig. 11a indicates that the droplets starting near the center of the jet may rebound from the target surface and re-impact more than once on the target surface while the droplet starting near the edge of the jet may never reach the target surface. Due in part to those multiple contacts of rebounding droplets, there are local peaks in droplet impact. Not shown, but notable, is the fact that the impact velocity ratio to injection velocity varies from 0.1 at 10 m/s to 0.5 at 30 m/s. On the other hand, 5 μm droplets do not strike the surface. This computational result supports authors' earlier hypothesis that these peaks of droplet impact density contribute to the off-axis maximum cooling observed in the experiment for some conditions because, as mentioned in Section 2, it has been shown that the enhancement results primarily from heat transfer to individual droplets as they contact the surface. Therefore, higher droplet impact density will lead to higher cooling.

4.2.1. Comparison between in-line and off-line data

For steam-only flow, the h-values at $x/d = 0$ and 1 of off-line points (○ symbol) are only slightly higher than those (▽ symbol) at in-line data. For mist/steam cases, h-values at $x/d = 1$ are higher at the in-line location than at off-line location (except for the case in Fig. 7). This can be caused by lower particle density at off-line locations because they are further away from the location, $x/d = 1$, where the mist has the most powerful effect. The distance between the off-line point at $x/d = 1$ and the jet center is $1.414d$. However, it is not clear why there is an exception in Fig. 7.

4.3. Relevance to real gas turbine application

Conditions in actual gas turbines will extend to higher pressures of about 30 bar, smaller dimensions, and about equal velocity so that the Reynolds numbers should be about 20–30 times larger. The surface temperature is also expected to be much higher, challenging the integrity of the material. The trends of this experiment are not considered limiting by any mechanism to prohibit successful application under such conditions. Besides, under real

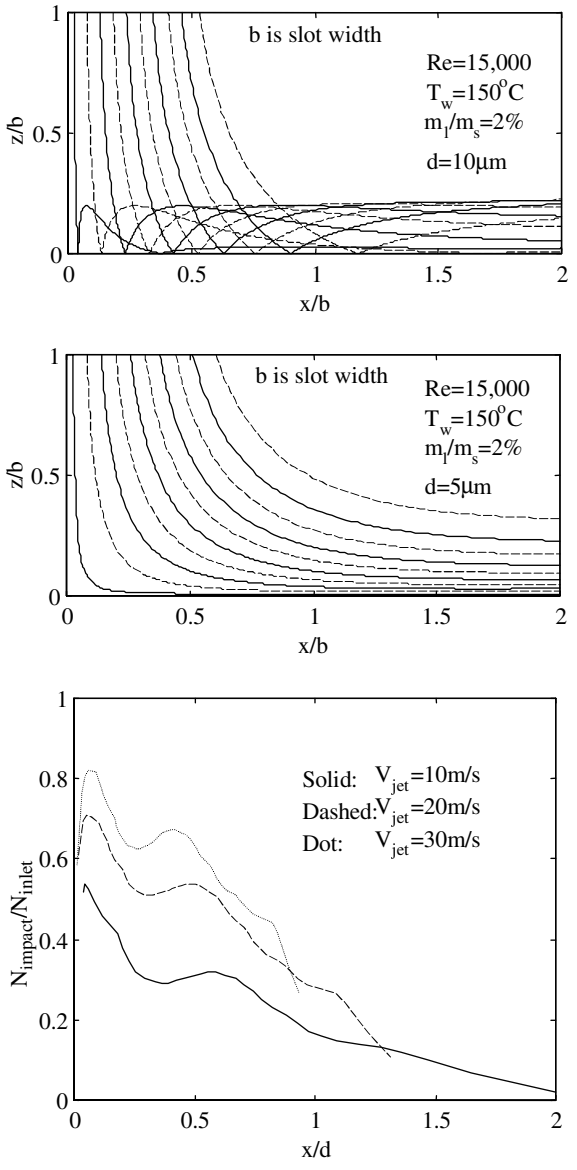

Fig. 11. 2-D computational results of impact density for 10 μm droplets.

engine conditions, the steam density will increase approximately 14 times while the liquid density will decrease approximately 15%. Heavier steam could sustain more volume of the liquid droplets, so this would translate into an increase of approximately 16 times more liquid volume (or more droplets) in the high-pressure engine condition with the same amount of liquid/steam mass ratio and liquid droplet size distributions as in the laboratory. More droplets would imply better cooling. Other favorable changes at real engines conditions include 2.8 times better steam thermal conductivity and 10% better steam specific heat C_p. Unfavorable changes include 24% re-

duction of latent heat and 100% increase of steam dynamic viscosity. Future studies are required to verify the validity of mist/steam heat transfer enhancement in high-temperature and high-pressure conditions. Care is needed to harness the cooling enhancement demonstrated in this study because the enhancement is limited to a few diameters near the impact zone. Future studies of multiple rows of jets with separation distance within 3–4 jet diameter are recommended.

5. Conclusions

When added to a steam flow impinging onto a heated, enclosed surface, mist enhances the rate of cooling by depressing the surface temperature. For a row of jets spaced at 3 diameters and spaced 2.8 diameters from a heated surface, the following conclusions are offered. For jet Reynolds numbers of 7500–22,500, heat fluxes of 3.3–13.4 kW/m^2 and mist contents ranging from 0.75% to 3.5%, the stagnation point enhancement, defined as the ratio of heat transfer coefficient with mist to that without, ranges from 50% to over 600%. The enhancement wanes away from the jet impingement and becomes negligible at about three jet diameters distant. The enhancement is relatively higher at lower heat flux.

The point of maximum temperature depression is observed for some conditions to lie off the stagnation point. Trajectory calculations suggest that droplet spreading and multiple contacts are expected. These effects tend to promote maximum cooling away from the impingement center, qualitatively.

Comparison of a slot jet and the row of discrete jets with equal mass flows indicate the slot achieves less cooling effectiveness in steam-only flow but produces superior cooling enhancement in mist/steam flow. The ability of liquid mist to offer augmented cooling of heated surfaces suggests the application to blade cooling for advanced turbines has merit from a cooling standpoint.

Acknowledgements

The authors would like to thank Graver Separations (Wilmington, DE) for donating the steam filters for the experiment. We also want to thank Mee Industries Inc. (El Monte, CA) for donating the pressure atomizers and the high-pressure pump. We appreciate the help from T. Guo in setting up the test facility. This research is sponsored by the US Department of Energy under the contract DOE/AGTSR 95-01-SR-034, and is managed by Dr. Larry Golan at the South Carolina Institute for Energy Studies.

Appendix A

To make comparison between different cases easily, Fig. A.1 presents the heat transfer results in Nusselt number. Only the results along the circle line between the jets in Fig. 1 are shown for clarity. It can be found that the Nusselt number for single-phase steam-only

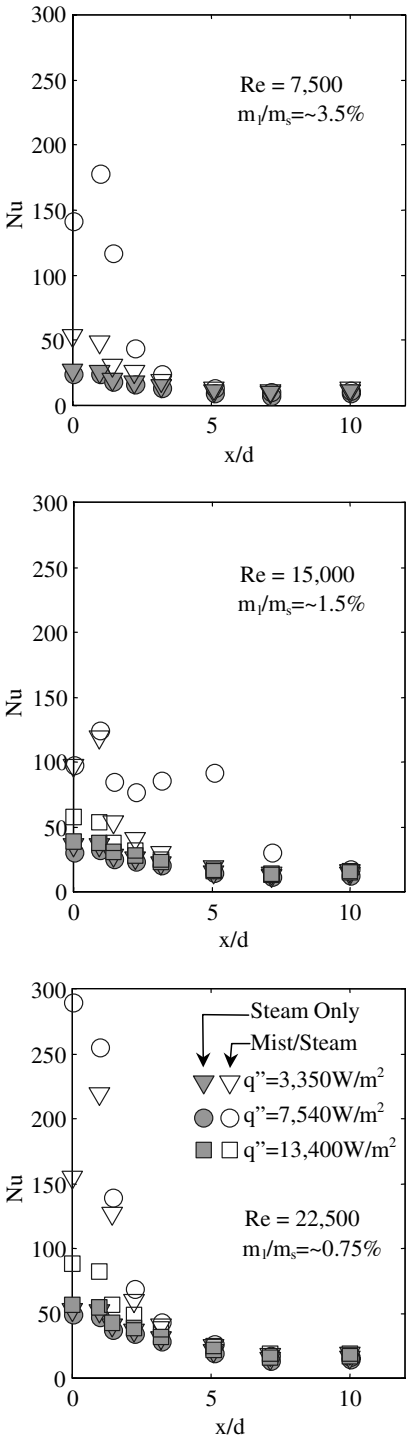

Fig. A.1. Heat transfer results in Nusselt number (only data along the circle line in Fig. 1).

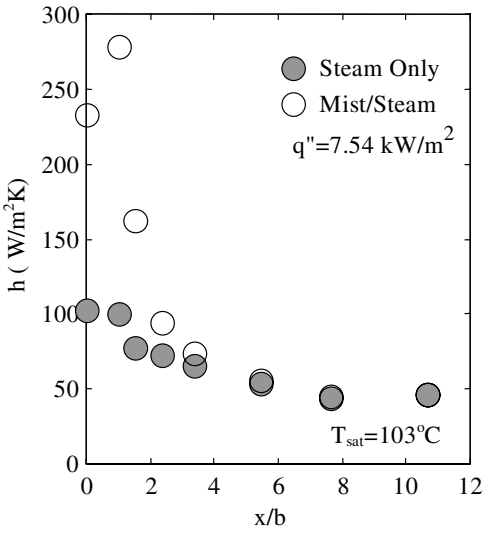

Fig. A.2. Heat transfer coefficient in a slot jet at $Re = 7500$ and $m_l/m_s = \sim 3.5\%$. Part of Fig. 7 in Li et al. [3].

flow collapses closely to the same curve under one Reynolds number while the results for mist/steam flow are affected significantly by the Reynolds number, mist concentrations and heat flux. The conclusions based on Nusselt number are identical with those based on heat transfer coefficient. Fig. A.2 is the heat transfer results of a slot jet obtained from Li et al. [3].

References

[1] T. Guo, T. Wang, J.L. Gaddis, Mist/steam cooling in a heated horizontal tube, part I: experimental system and part II: results and modeling, ASME J. Turbomachin. 122 (2000) 360–374.

[2] T. Guo, T. Wang, J.L. Gaddis, Mist/steam cooling in a 180° tube bend, ASME J. Heat Transfer 122 (2001) 749–756.

[3] X. Li, J.L. Gaddis, T. Wang, Mist/steam heat transfer in confined slot jet impingement, ASME J. Turbomachin. 123 (2001) 161–167.

[4] N.V. Nirmalan, J.A. Weaver, L.D. Hylton, An experimental study of turbine vane heat transfer with water–air cooling, ASME J. Turbomachin. 120 (1998) 50–62.

[5] M.J. Goodyer, R.M. Waterston, Mist-cooled turbines, in: Conf. of Heat and Fluid Flow in Steam and Gas Turbine Plant, Proc. Inst. Mech. Eng. (1973) 166–174.

[6] T. Takagi, M. Ogasawara, Some characteristics of heat and mass transfer in binary mist flow, In: Proc. of 5th Int. Heat Transfer Conf., Tokyo, 1974, pp. 350–354.

[7] K. Mastanaiah, E.N. Ganic, Heat transfer in two-component dispersed flow, J. Heat Transfer 103 (1981) 300–306.

[8] H. Fujimoto, N. Hatta, Deformation and rebounding processes of a water droplet impinging on a flat surface above leidenfrost temperature, J. Fluids Eng. 118 (1996) 142–149.

[9] T. Wang, J.L. Gaddis, X. Li, Mist/steam cooling for advanced gas turbine systems—Volume 3. Cooling by a Mist/Steam Jet, Final report to Advanced Gas Turbine Systems Research, South Carolina Institute of Energy Studies, US DOE contract No. DE-FC21-92MC29061, 2000.

[10] X. Li, J.L. Gaddis, T. Wang, Modeling of heat transfer in a mist/steam impinging jet, ASME J. Heat Transfer 124 (2001) 1086–1092.

[11] H. Yoshida, K. Suenaga, R. Echigo, Turbulence structure and heat transfer of a two-dimensional impinging jet with gas–solid suspensions, NHTC 2 (1998) 461–467.

[12] Y.A. Buyevich, V.N. Mankevich, Interaction of dilute mist flow with a hot body, Int. J. Heat Mass Transfer 38 (1995) 731–744.

[13] N. Hatta, H. Fujimoto, K. Kinoshita, H. Takuda,, Experimental study of deformation mechanism of a water droplet impinging on hot metallic surfaces above leidenfrost temperature, J. Fluids Eng. 119 (1997) 692–699.

[14] Fluent, FLUENT 4.4 User's Guide, I–III, Fluent Inc., 1997.

[15] Y.A. Buyevich, V.N. Mankevich, Cooling of a superheated surface with a jet mist flow, Int. J. Heat Mass Transfer 39 (1996) 2353–2362.

[16] X. Li, Cooling by a mist/steam jet, PhD Dissertation, Clemson University, SC, 1999.

[17] R.J. Moffat, Using uncertainty analysis in the planning of an experiment, J. Fluids Eng. 107 (1985) 173–178.